RESEARCH ARTICLE

Quantifying floridean starch storage patterns in Arctic rhodoliths: blue carbon implications

Milane Gabsteiger,[1] Ines Pyko,[1] Max Wisshak[2] & Sebastian Teichert[1]

[1]GeoZentrum Nordbayern, Friedrich-Alexander-Universität Erlangen-Nürnberg (FAU), Erlangen, Germany; [2]Marine Research Department, Senckenberg am Meer, Wilhelmshaven, Germany

Abstract

Rhodoliths composed of crustose coralline algae (CCA) are marine calcifiers of global significance. Here, we investigate how floridean starch storage patterns of Arctic rhodoliths from Svalbard are affected by environmental conditions. Quantifying the amount of starch in photomosaic scans of rhodolith slabs via amylopectin–iodine complex formation, we found that shallow water rhodoliths contain significantly higher starch percentages compared to the deeper-water dwellers. We conclude that the observed starch patterns are mainly controlled by water depth because light and rhodolith turnover frequency both decrease in deeper waters. Regarding rhodolith turnover, the occasional burial of turned rhodoliths in deeper waters can result in a dieback of the outer CCA thallus areas, which contain important starch supplies. As rhodoliths are both calcifiers and photoautotrophs, we highlight their relevance in potentially contributing to global blue carbon, that is, their role as a marine carbon sink. In this context, our quantification approach of floridean starch patterns in rhodoliths provides a straightforward basis for further studies on this topic.

Keywords

Crustose coralline algae; depth gradient; Svalbard; marine carbon sink; calcifiers; *Boreolithothamnion glaciale*

Correspondence

Sebastian Teichert, GeoZentrum Nordbayern, Friedrich-Alexander-Universität Erlangen-Nürnberg, Loewenichstraße 28, DE-91054 Erlangen, Germany. E-mail: sebastian.teichert@fau.de

Abbreviations

CCA: crustose coralline algae
CTD: conductivity–temperature–depth instrument
PAR: photosynthetically active radiation

To access the supplementary material, please visit the article landing page

Introduction

CCA are globally occurring macroalgae from the subclass Corallinophycidae that are abundant from the tropics to polar latitudes in 0–290 m water depth (Littler et al. 1985; López Correa et al. 2023; Teichert 2024) and with a fossil record dating back to the Paleozoic (Riding et al. 1998; Teichert et al. 2019). CCA mainly inhabit marine ecosystems but also have been found in freshwater environments (Ragazzola et al. 2020). CCA can grow attached to a fixed substratum such as bedrock or coral reefs or unattached and free-living, such as broken-off thalli that continue to grow; they can also completely envelope small stones or other nuclei (Woelkerling 1988). As soon as the fraction of CCA material within such a structure exceeds the 50% benchmark, it is called a rhodolith (Bosence 1983), which may contain other calcifying organisms in varying fractions (Pyko et al. 2025). Regardless of their development as fixed crusts or rhodoliths, CCA fulfil important roles as ecosystem engineers in a great variety of environments (Teichert, Steinbauer et al. 2020; Tuya et al. 2023; Straube et al. 2024). The thallus of CCA features calcification in the form of calcite with a varying incorporation of magnesium (Nash et al. 2011; Smith et al. 2012; Teichert, Voigt et al. 2020). The calcite is precipitated within the cell walls, which is spatially controlled by a polysaccharide matrix, mainly made up of sulphated galactans, linear polymers consisting of alternating residues of the 3-linked β-galactose and a 4-linked α-galactose (Bilan & Usov 2001).

Additional to these structurally important polysaccharides, CCA and other red algae produce starch, one of the most important reserve materials in the plant realm. This so-called floridean starch is only composed of amylopectin-like molecules (α-1,4-linked glucose with branched α-1,6-linked glucose), in contrast to land plant starches that are composed of both amylose (linear α-1,4-linked glucose) and amylopectin (α-1,4-linked glucose with branched α-1,6-linked glucose; (Yu et al. 2002; Xue et al. 2021). Also, the average chain length of floridean starch is shorter than that of amylopectin in higher plants, such as potato amylopectin and maize amylopectin (Yu et al. 2002). Unlike chlorophytes, rhodophytes synthesize and store starch as granules outside their plastids in the

Citation: *Polar Research* 2025, *44*, 10992, http://dx.doi.org/10.33265/polar.v44.10992

cytosol (Pueschel 1990), in cells below the layer of meristem cells (Giraud & Cabioch 1983), and their development is associated with the endoplasmic reticulum (Borowitzka 1978). There is not much information on the regulation of photosynthetic carbon allocation in red algae; however, floridean starch represents the major sink for photosynthetically fixed carbon in Rhodophyta (Viola et al. 2001).

The role of floridean starch as a reserve material in red algae becomes especially evident in environments with short vegetation periods, as is characteristic for polar latitudes. One of the most common CCA species in this context is *Boreolithothamnion glaciale* (Kjellman) (Gabrielson et al. 2023) (basionym *Lithothamnion glaciale* Kjellman 1883) in the High-Arctic Svalbard archipelago. Here, the species experiences several months of darkness because of sea-ice formation and the polar night (Teichert & Freiwald 2014). It has been recognized in preliminary experiments (Teichert 2013) to contain starch (Fig. 1). During the short summer period, *B. glaciale* stores photosynthetically derived floridean starch within its perithallial tissue. During the winter, the carbon is utilized to allow the organism to survive the approximately 120 days of polar night (Freiwald & Heinrich 1994). Wiencke et al. (2009) have demonstrated a similar seasonal pattern for the Arctic kelp *Laminaria solidungula*. So, while it is well-known that CCA and other algae can thrive in polar environments, the role of floridean starch for CCA in this context has been tackled only superficially (Freiwald & Henrich 1994).

Along the coasts of Svalbard, *B. glaciale* can be found as crusts on fixed substrates but mainly occurs in the form of unattached rhodoliths that are mostly at depths between 11 m and 47 m, though they can be found in the dysphotic zone as far down as 81 m (Teichert et al. 2014; Wisshak et al. 2017; Wisshak et al. 2019). As rhodoliths are unattached, they can be turned around by water movement or organisms in search of food (Wisshak et al. 2019), thus altering the orientation of a rhodolith towards incident light. Both factors—the water depth in which a specific rhodolith thrives as well as its orientation on the seafloor—are potential prerequisites for the production of floridean starch, whose quantitative distribution within rhodoliths and CCA in general has not been analysed before.

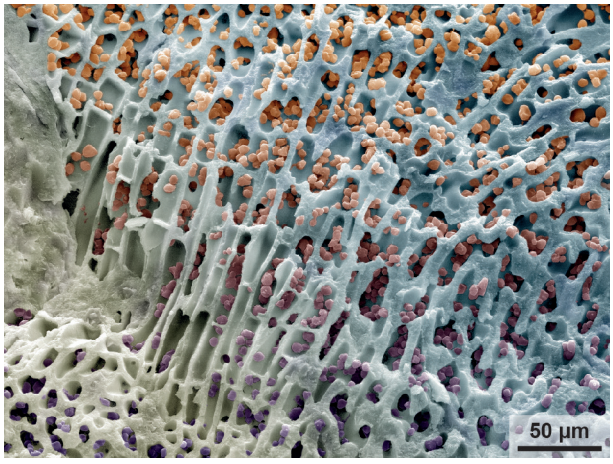

Fig. 1 A digitally coloured scanning electron microscopy image (colour values do not represent analytical information) of starch grains distributed in the calcified thallus of *Boreolithothamnion glaciale* collected at 46 m water depth in Mosselbukta, Svalbard.

Deciphering some of the mechanisms that govern starch production and distribution in CCA would also improve our understanding of their role in blue carbon, that is, carbon burial in the marine realm (Krause-Jensen et al. 2018). It has been suggested that this role might be significant (van der Heijden & Kamenos 2015); however, there are many unknowns, especially over longer timescales (Mao et al. 2020). Quantifying the contribution of CCA to blue carbon is particularly complicated because, as calcifying organisms, CCA also contribute to calcification-driven CO_2 emissions (Van Dam et al. 2021). Starch, as a relatively stable polysaccharide (Yu et al. 2021) with a high potential for long-term burial, is an important variable in this equation.

In this study, we employed iodine staining on rhodolith serial cross-sections to quantify the amount of incorporated starch, using specimens mainly composed of the CCA species *B. glaciale* that had been collected at different water depths. We hypothesized that (1) the starch content of the rhodoliths would decrease with water depth because deep-water specimens receive less light and are moved less frequently and (2) that the starch content would be higher in the top parts of a rhodolith because the scattered light in the water column reaches the bottom parts of the rhodoliths less extensively than the top parts.

Material and methods

Study area

The rhodolith samples were obtained during the MSM 55 expedition (ARCA) of the RV *Maria S. Merian* from 11 to 29 June 2016 (Wisshak et al. 2017) in Mosselbukta. Located at the mouth of the fjord Wijdefjorden, Spitsbergen, the bay of Mosselbukta is 5 km long and up to 8 km wide (79°53′N, 15°55′E). Mosselbukta is a classical site for geo-biological research on carbonate production by benthic communities in Svalbard waters and was first surveyed by Kjellman (1883), who reported

Citation: *Polar Research* 2025, *44*, 10992, http://dx.doi.org/10.33265/polar.v44.10992

rhodolith beds several square kilometres in extent. These were further characterized by Teichert et al. (2014) and the carbonate production rates of the beds were assessed by Teichert & Freiwald (2014), who found that the beds appear most pronounced at around 45 m water depth, with a production rate of 119.8 g ($CaCO_3$) m^{-2} yr^{-1}, where rhodoliths of up to 25 cm in diameter cover 60–80% of the seafloor. Glaciogenic material—from pebble to boulder sized stones—dominates the seafloor in Mosselbukta, providing suitable hardground for CCA and subsequent rhodolith formation. *Boreolithothamnion glaciale* is the prevailing CCA species and can be encountered down to the dysphotic depth of 81 m (Teichert et al. 2014; Wisshak et al. 2017).

Its polar latitude subjects Mosselbukta to extreme seasonality. Although there are no permanently moored data logging stations in the area, environmental data from repeated CTD profiling, autonomous temperature and salinity logging (over 15 months) and short-term lander deployments reveal several distinct water masses affecting the area over the course of the year (Wisshak et al. 2019). Sea-ice cover varies in Mosselbukta but commonly forms in December/January and starts to break up between May and July (Spreen et al. 2008), minimizing the PAR significantly during that time. Daylight is absent during the polar night, which lasts 122 days at Mosselbukta (NOAA 2023). Generally, the PAR levels at 46 m water depth are low, with only a few measurements above the detection limit recorded during a short-term lander deployment, reaching a maximum of only 4.5 µmol m^{-2} s^{-1} (Wisshak et al. 2019). Measurements in 2006 indicated that the rhodoliths at this site thrive under dysphotic conditions with less than 1% surface irradiance (Teichert et al. 2014).

Rhodolith collection and preparation

Using the manned submersible *Jago*, two rhodoliths were collected from a shallow-water (12.7 m) and two from each of two deeper-water (46.8 and 48.8 m) locations in Mosselbukta (Table 1, Fig. 2). Collected rhodoliths were dried in cabinet desiccators at 30°C for 48 hours onboard the research vessel and stored in sealed plastic bags containing silica gel as a drying agent. All sampled rhodoliths were mainly built by the CCA species *B. glaciale*. Species identification was based on works by Adey (1970) and Gabrielson et al. (2023), supplemented by notes by Teichert et al. (2014).

In the laboratory, complete rhodoliths were embedded in Water-clear+ (RG Faserverbundwerkstoffe GmbH) epoxy resin, which has a resin to hardener ratio of 100:35. After air-drying for 48 hours, the rhodoliths were sectioned vertically with a Buehler low-speed, water-cooled diamond rock saw to produce slabs of ca. 1.5 cm thickness, resulting in different amounts of cross-cut surfaces for later analysis (Table 1). The different amounts of slabs depended on the rhodoliths' sizes and are unproblematic for the statistical analysis. Each slab surface was then coated with another thin layer of epoxy resin for stabilization, air-dried for 48 hours and polished with silicon carbide suspensions of grain sizes down to P800 to remove all the material that was covered with the stabilizing resin.

Starch quantification

The starch–iodine reaction (Colin & Gaultier de Claubry 1814) was used to quantify the starch content in the rhodoliths. While this reaction has been used to visualize floridean starch in rhodoliths before (Fredericq et al. 2019), it is important to note that colouration following iodine treatment works differently for floridean starch than for the starch of other plants, like potatoes. The deep blue colour known from iodine-treated potato starch—with an absorbance peak of 590 nm and a blue value of 0.49 (Yu et al. 2002)—derives from a complex formation with amylose (Saenger 1984), which is not present in floridean starch. The amylopectin–iodine complex formed in floridean starch (Davis et al. 1994) is characterized by a red to purple colour that has an absorbance peak of 527–530 nm and a blue value of 0.10 (Yu et al. 2002). The colour change to this purple is a straightforward method to track floridean starch in rhodoliths, which we utilized.

Before staining, each slab surface was photographed at 25× magnification with a Zeiss Axio Zoom.V16 microscope equipped with a Zeiss Axiocam 506, using the tile stitching mode operated by the Zeiss ZEN core software. This was done to get a record of the untreated slab surfaces for later comparison with the stained specimens.

For iodine staining, each slab surface was immersed in Lugol's solution (iodine–potassium iodide solution) for three minutes, rinsed with demineralized water for five seconds and dried with compressed air. Immediately thereafter, each slab was again photographed. Considering all areas that gained a red to purple colour (in contrast to the untreated version) as containing floridean starch, we used ImageJ Fiji version 2.9.0 (Schindelin et al. 2012) to calculate the ratio between the complete CCA area and the portion that contained floridean starch. We did not employ automatic measurements (i.e., based on colour mapping) but assigned the areas of starch measurements manually in order to avoid misinterpretations. Additionally, each rhodolith slab was divided into a top and a bottom part, depending on the position of the rhodolith on the seafloor at the time of collection, and

Table 1 Overview of rhodolith samples.

Rhodolith no.	Analysed surfaces (*n*)	Sampling station	Water depth (m)	Latitude	Longitude
10064b	6	MSM55/442	12.7	79°54.41' N	15°54.85' E
10064c	8	MSM55/442	12.7	79°54.41' N	15°54.85' E
10353	8	MSM55/416-1	46.6	79°54.69' N	15°48.61' E
10365	8	MSM55/433-1	48.8	79°54.33' N	15°47.82' E

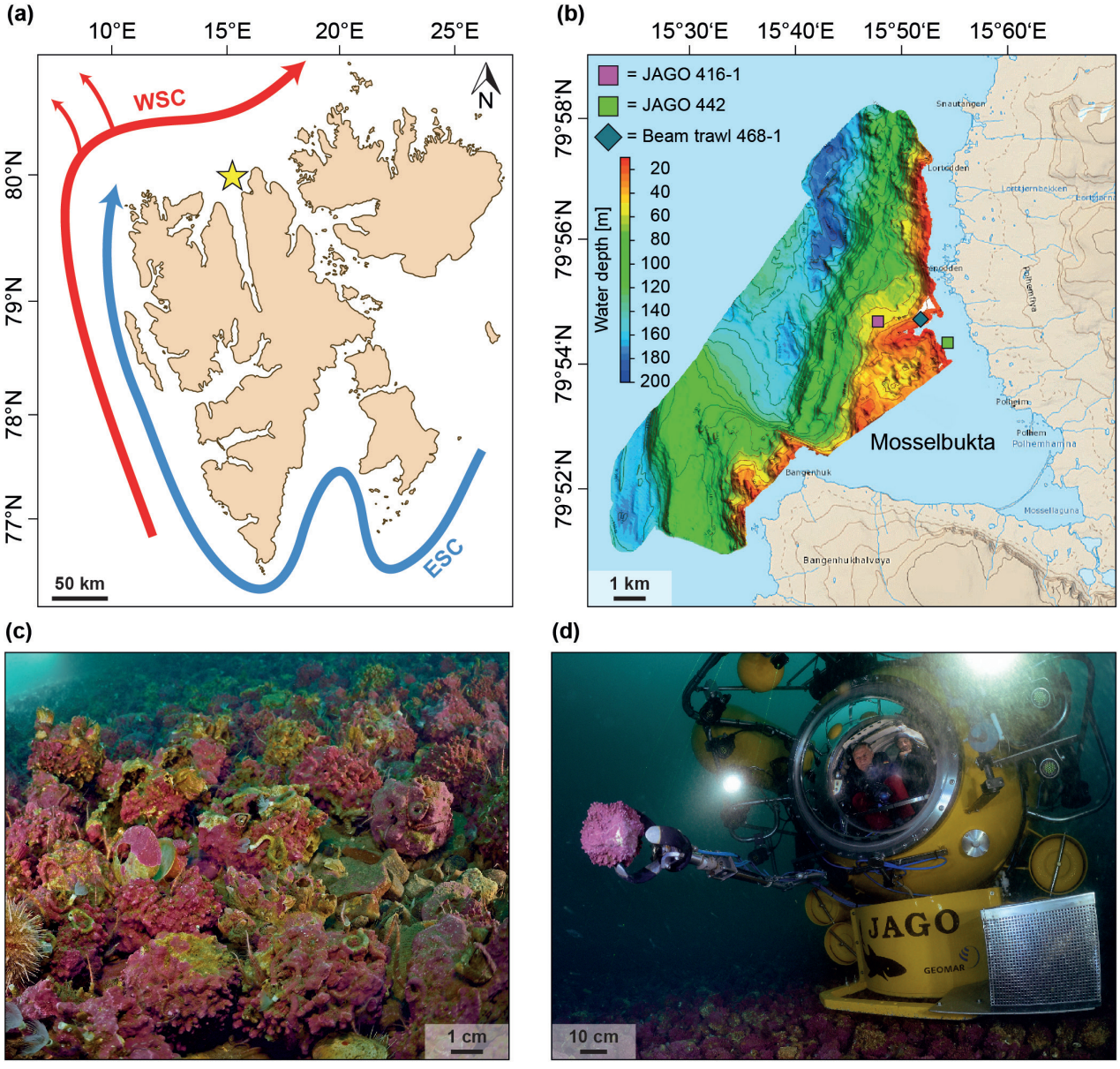

Fig. 2 Study area and rhodolith sampling sites. (a) Location of the study area Mosselbukta in northern Spitsbergen, Svalbard. Arrows indicate the main ocean currents: the warm West Spitsbergen Current (WSC) and the cold East Spitsbergen Current (ESC). (b) Multibeam map of Mosselbukta, indicating the three rhodolith sampling sites and the gear used (topographic map extract is used by courtesy of the Norwegian Polar Institute). (c) Rhodolith bed in 40 m water depth at Mosselbukta (photo: Solvin Zankl). (d) Rhodolith sampling via the manned *Jago* submersible (photo: Solvin Zankl).

Citation: *Polar Research* 2025, *44*, 10992, http://dx.doi.org/10.33265/polar.v44.10992

separate quantifications were made for both halves. This was possible because the top parts still showed the reddish colour typical of CCA while the bottom parts were bleached, potentially due to CCA dieback or at least photosynthetic inactivity (Schlüter et al. 2021). We also wanted to quantify the starch content on the basis of the complete rhodoliths, so we ended up with the following data: top rhodolith matrix area; bottom rhodolith matrix area; complete matrix area; top rhodolith starch area; bottom rhodolith starch area; and complete starch area. All measurements were in mm^2.

To quantify how deep floridean starch is stored in the algal thallus, we measured the thickness of starch-coloured areas at 10 spots for each slab randomly, including branch tips and sides, not distinguishing between top and bottom parts of the rhodoliths. The complete approach to visualize and measure the starch-containing rhodolith areas as well as the division between top and bottom rhodolith parts and the depths of starch storage is visualized in Fig. 3.

Statistical approach

Statistical analyses were performed in R version 4.3.1 (R Core Team 2023) and PAST4 (Hammer et al. 2001). We calculated the starch:matrix ratios for the top and bottom parts of each rhodolith by dividing the starch areas by the respective matrix areas of the slabs and calculating the mean ratio and standard deviations. Then, we summed up starch areas from top and bottom and divided it by the summed-up matrix areas to obtain the starch:matrix ratios for the complete rhodoliths.

Starch:matrix ratios divided into top and bottom areas as well as ratios for the complete rhodoliths were tested for normal distribution using the Shapiro–Wilk test. As some of the data in both data sets were not normally distributed, we used non-parametric tests for further analysis.

To infer if there are significant differences in the starch:matrix ratios between the top and bottom parts of each rhodolith, we used the Wilcoxon signed rank test, a two-sample paired test that accounts for the fact that top and bottom starch:matrix ratios derive from individual rhodolith slabs. The results were visually complemented by box plots.

To infer if there is a significant difference in the starch:matrix ratios between deep and shallow water rhodoliths, we employed a Kruskal–Wallis test to check if there is a significant difference between groups (main effect) and Mann–Whitney pairwise post hoc tests to conduct pairwise comparisons amongst groups.

To quantify how deep floridean starch is stored in the algal thallus, we measured the thickness of starch-coloured areas at 10 spots for each rhodolith slab randomly, resulting in 60 measurements for rhodolith 10064b and 80 measurements for rhodoliths 10064c, 10365 and 10353. Mean starch thicknesses for each rhodolith were tested for normal distribution using the Shapiro–Wilk test. Potential differences between groups (water depth) were tested with the non-parametric Kruskal–Wallis test and Dunn's post hoc test.

Potential clusters based on calculated starch:matrix ratios across all samples were analysed and identified using the clustering algorithm K-Mean (MacQueen 1967). K-means clustering requires a predefined number of clusters, which was determined and visualized with the function fviz_nbclust() in the "factorextra" R package (Kassambara & Mundt 2020), using the within-cluster sums of squares and average silhouette. Additionally, the function fviz_gap-stat() in the "factorextra" R package was used to visualize the gap statistics generated by the function clusGap() in the "cluster" R package (Maechler et al. 2023). After specifying the optimal number of clusters, the K-Means cluster analysis was performed with the function kmeans() in the "stats" R package (R Core Team 2023). As recommended, nstart was set to >1 (25). Clustering results were plotted with the function fivz_cluster() in the "factorextra" R package.

Results

For all analysed slab surfaces, the resulting matrix and starch areas, the corresponding ratios and the calculated mean values for each rhodolith are compiled in Table 2. The Shapiro–Wilk test indicated normal distribution for all data except the top part of rhodolith 10365 and for the complete rhodolith 10064c (Table 3), so we continued with non-parametric tests for the complete data set. Results of the Wilcoxon signed rank test on the starch:matrix ratios of top and bottom rhodolith parts indicated that differences are significant in half of the samples (Table 4, Fig. 4a), where the ratios were always higher in the top than in the bottom parts. For the complete rhodoliths, the Kruskal–Wallis test indicated a significant difference between the starch:matrix ratio sample means of the complete rhodoliths ($H_\chi^2 = 19.84$, $p = 0.00018$) and the Mann–Whitney pairwise post hoc tests indicated differences between rhodoliths from deep and shallow waters (Table 5, Fig. 4b).

Measured starch thicknesses reveal that starch is located not only at the surface of the CCA but up to several millimetres deep in the skeleton. Raw data show that the mean ratios from shallower waters are higher than the mean ratios from deeper waters (Fig. 5). Data are not normally distributed (Table 6). The Kruskal–Wallis test indicated that there is a significant difference between the

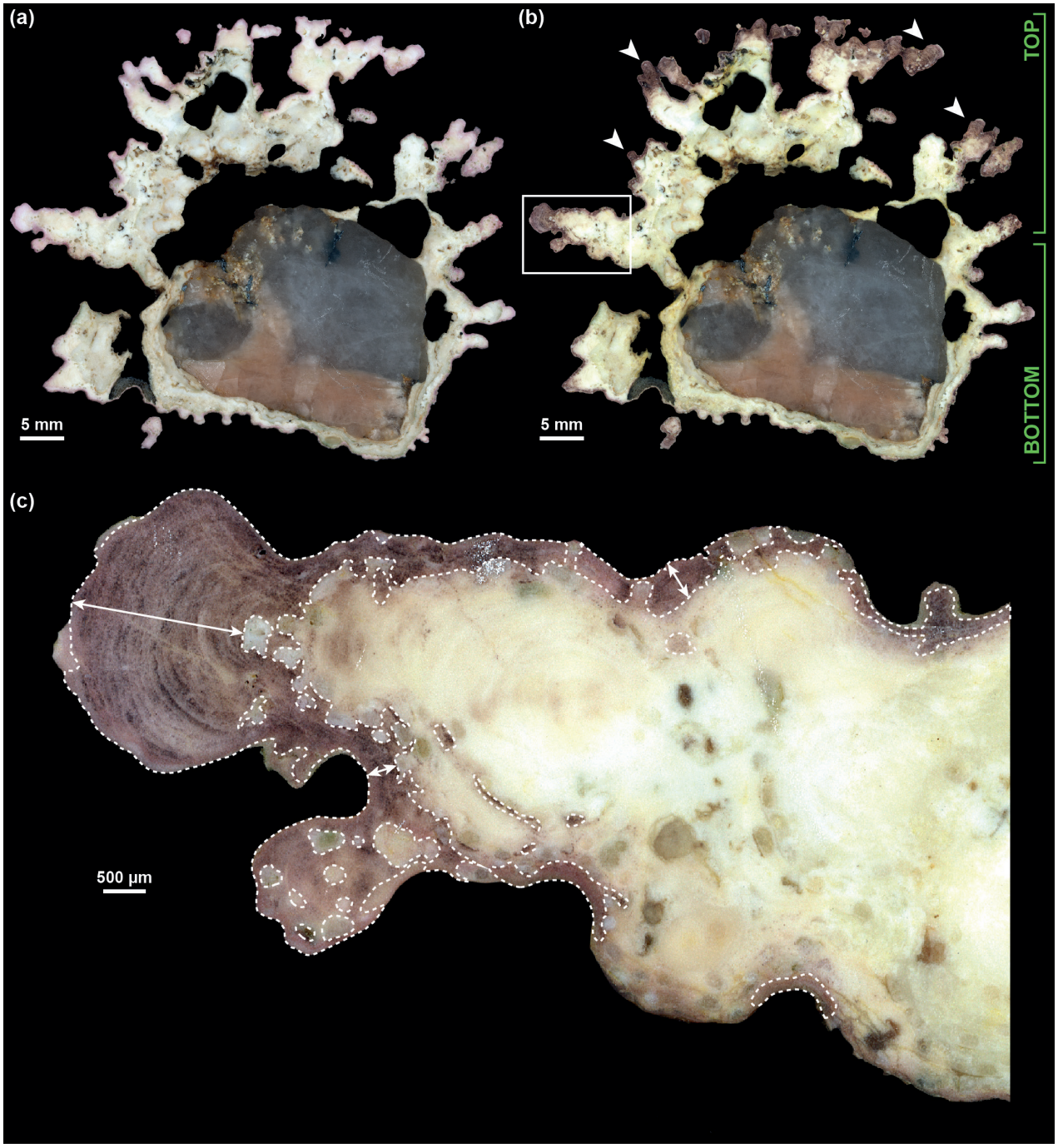

Fig. 3 Starch quantification: (a) Rhodolith slab before treatment with Lugol's solution; (b) after treatment, with areas containing starch coloured red to purple (white arrows), including division in top and bottom parts, indicated by green brackets; white rectangle indicates (c) close-up image of starch area measurement (indicated by white dashed line) and starch storage depth measurements (indicated by white double arrows; the long arrow represents a branch tip measurement, short arrows represent branch side measurements) in ImageJ Fiji.

median starch thicknesses ($H_{\chi}^{2} = 99.2$, $p < 0.0001$). The Dunn's post hoc exact test indicates significant differences only between rhodoliths from different water depths and not between rhodoliths from the same water depth (Table 7). Nevertheless, these data need to be considered conservative because, while the depth measurements were distributed randomly over the rhodolith, many areas remain uncovered. Moreover, it would be necessary

Citation: *Polar Research* 2025, *44*, 10992, http://dx.doi.org/10.33265/polar.v44.10992

Table 2 Rhodolith starch content for each slab surface and rhodolith mean values (values in boldface are means ± standard deviation), divided into top and bottom parts and for the complete rhodoliths.

Slab surface or rhodolith no.	Water depth (m)	Rhodolith matrix area top (mm^2)	Rhodolith starch area top (mm^2)	Starch:matrix ratio top	Rhodolith matrix area bottom (mm^2)	Rhodolith starch area bottom (mm^2)	Starch:matrix ratio bottom	Rhodolith matrix area (mm^2)	Rhodolith starch area (mm^2)	Starch:matrix ratio complete
10064b-1	12.7	541.6	103.0	0.190	523.6	56.4	0.108	1065.2	159.4	0.150
10064b-2.1	12.7	514.4	78.4	0.152	725.9	37.7	0.052	1240.3	116.1	0.094
10064b-2.2	12.7	518.8	115.8	0.223	318.9	32.8	0.103	837.7	148.6	0.177
10064b-3.1	12.7	553.0	143.5	0.259	429.8	52.6	0.122	982.8	196.1	0.200
10064b-3.2	12.7	467.0	124.8	0.267	323.9	29.2	0.090	790.9	154	0.195
10064b-4	12.7	348.0	130.3	0.374	451.6	19.3	0.043	799.6	149.6	0.187
10064b	**12.7**	**490.5 ± 75.8**	**116.0 ± 22.9**	**0.244 ± 0.077**	**462.3 ± 151.1**	**38.0 ± 14.2**	**0.074 ± 0.035**	**952.7 ± 178.4**	**154.0 ± 25.6**	**0.167 ± 0.040**
10064c-1	12.7	191.4	23.0	0.120	163.8	29.7	0.181	355.2	52.7	0.148
10064c-2.1	12.7	394.9	103.9	0.263	326.2	113.0	0.346	721.1	216.9	0.301
10064c-2.2	12.7	608.4	50.6	0.083	131.4	41.7	0.317	739.8	92.3	0.125
10064c-3.1	12.7	589.4	70.8	0.120	89.2	27.3	0.306	678.6	98.1	0.145
10064c-3.2	12.7	737.1	46.2	0.063	150.8	43.5	0.288	887.9	89.7	0.101
10064c-4.1	12.7	813.2	63.3	0.078	161.2	33.3	0.207	974.4	96.6	0.099
10064c-4.2	12.7	597.6	77.8	0.130	425.4	39.6	0.093	1023	117.4	0.115
10064c-5	12.7	267.2	61.6	0.231	391.7	42.7	0.109	658.9	104.3	0.158
10064c	**12.7**	**524.9 ± 220.1**	**62.2 ± 23.9**	**0.136 ± 0.073**	**230.0 ± 130.1**	**46.4 ± 27.6**	**0.231 ± 0.097**	**754.9 ± 211.8**	**108.5 ± 47.5**	**0.149 ± 0.065**
10365-1	48.8	208.1	27.4	0.132	211.3	23.9	0.113	419.4	51.3	0.122
10365-2.1	48.8	260.3	39.5	0.152	279.2	14.9	0.053	539.5	54.4	0.101
10365-2.2	48.8	263.0	1.3	0.005	144.5	14.0	0.097	407.5	15.3	0.038
10365-3.1	48.8	178.2	0.9	0.005	126.6	18.1	0.143	304.8	19	0.062
10365-3.2	48.8	232.2	0.4	0.002	136.4	8.3	0.061	368.6	8.7	0.024
10365-4.1	48.8	213.2	0.8	0.004	117.9	5.0	0.042	331.1	5.8	0.018
10365-4.2	48.8	326.3	0.0	0.000	198.6	0.0	0.000	524.9	0	0.000
10365-5	48.8	384.5	0.0	0.000	248.9	0.0	0.000	633.4	0	0.000
10365	**48.8**	**258.2 ± 67.9**	**8.8 ± 15.6**	**0.037 ± 0.065**	**182.9 ± 60.6**	**10.53 ± 8.7**	**0.064 ± 0.051**	**441.1 ± 114.1**	**19.3 ± 21.7**	**0.046 ± 0.046**
10353-1	46.6	287.3	14.9	0.052	368.9	2.3	0.006	656.2	17.2	0.026
10353-2.1	46.6	255.8	21.7	0.085	494.6	11.7	0.024	750.4	33.4	0.045
10353-2.2	46.6	402.0	23.6	0.059	270.8	7.7	0.028	672.8	31.3	0.047
10353-3.1	46.6	368.5	25.0	0.068	225.4	3.6	0.016	593.9	28.6	0.048
10353-3.2	46.6	367.0	13.0	0.035	187.1	5.4	0.029	554.1	18.4	0.033
10353-4.1	46.6	320.8	8.5	0.026	283.5	7.5	0.026	604.3	16	0.026
10353-4.2	46.6	612.3	26.7	0.044	454.8	3.8	0.008	1067.1	30.5	0.029
10353-5	46.6	635.2	19.1	0.030	364.8	5.1	0.014	1000	24.2	0.024
10353	**46.6**	**406.1 ± 142.4**	**19.1 ± 6.4**	**0.050 ± 0.020**	**331.2 ± 108.5**	**5.9 ± 3.0**	**0.019 ± 0.009**	**737.3 ± 192.9**	**24.9 ± 7.0**	**0.035 ± 0.010**

Table 3 Results of the Shapiro–Wilk test for normal distribution of data for the top-bottom divided and the complete rhodolith starch:matrix ratios.

	10064b top	10064b bottom	10064b complete	10064c top	10064c bottom	10064c complete	10365 top	10365 bottom	10365 complete	10353 top	10353 bottom	10353 complete
N	6	6	6	8	8	8	8	8	8	8	8	8
Shapiro–Wilk *W*	0.9518	0.9014	0.8299	0.8503	0.9050	0.7290	0.6146	0.9448	0.8917	0.9532	0.8944	0.8383
p (normal)	0.7546	0.3823	0.1074	0.0960	0.3200	0.0048	0.0002	0.6591	0.2427	0.7431	0.2567	0.0723
normal distribution	Yes	Yes	Yes	Yes	Yes	No	No	Yes	Yes	Yes	Yes	Yes

Table 4 Results of the Wilcoxon signed rank test on differences between the starch:matrix ratios of top and bottom rhodolith parts.

	10064b top/ bottom	10064c top/ bottom	10365 top/ bottom	10353 top/ bottom
N	6	8	8	8
W	21	31	15	36
p	<0.0277	0.0687	0.3454	0.0117
significantly different	Yes	No	No	Yes

to normalize starch storage data to cell size in further specialized studies to draw conclusions about the true distributional coverage within the CCA tissue.

K-means clustering resulted in an optimal number of three clusters (Fig. 6, Supplementary Fig. S1). Cluster visualization clearly shows one cluster containing almost all the calculated starch:matrix ratios from the deeper-water samples. The calculated starch matrix ratios from the shallow-water samples divide in two different clusters, which mostly represent the two rhodolith specimens.

Discussion

The influence of water depth

Our study focused on the starch:matrix ratios and starch localization in rhodoliths collected from different water depths in an Arctic environment. Rhodolith-forming CCA allocate carbon through photosynthesis, so we hypothesized that PAR is the most important factor in controlling starch production in CCA and, therefore, water depth has a significant influence on the storage of starch granules within the CCA tissue. Rhodolith-forming CCA have a low-light adapted photosystem (Gantt 1990), but our results suggest that as illumination decreases with water depth, it causes a decrease of starch production. At 12.7 m water depth, the rhodoliths are located inside the euphotic zone with an irradiance of about 10% of the surface illumination, while the samples from the deeper waters (46.6 m and 48.6 m) are located in the dysphotic zone and receive only ca. 1% of the surface illumination (Teichert et al. 2014). Supporting our hypothesis, all the statistical tests indicated a significant difference in the starch:matrix ratios associated with shallow- versus deep-water rhodoliths, with higher values in the samples from shallow water (maximum 37.4% starch content) and lower values in those from deeper waters (maximum 15.2% starch content). The significant decrease of starch infusion thicknesses in the CCA thallus with water depth underpins these assumptions.

Citation: *Polar Research* 2025, *44*, 10992, http://dx.doi.org/10.33265/polar.v44.10992

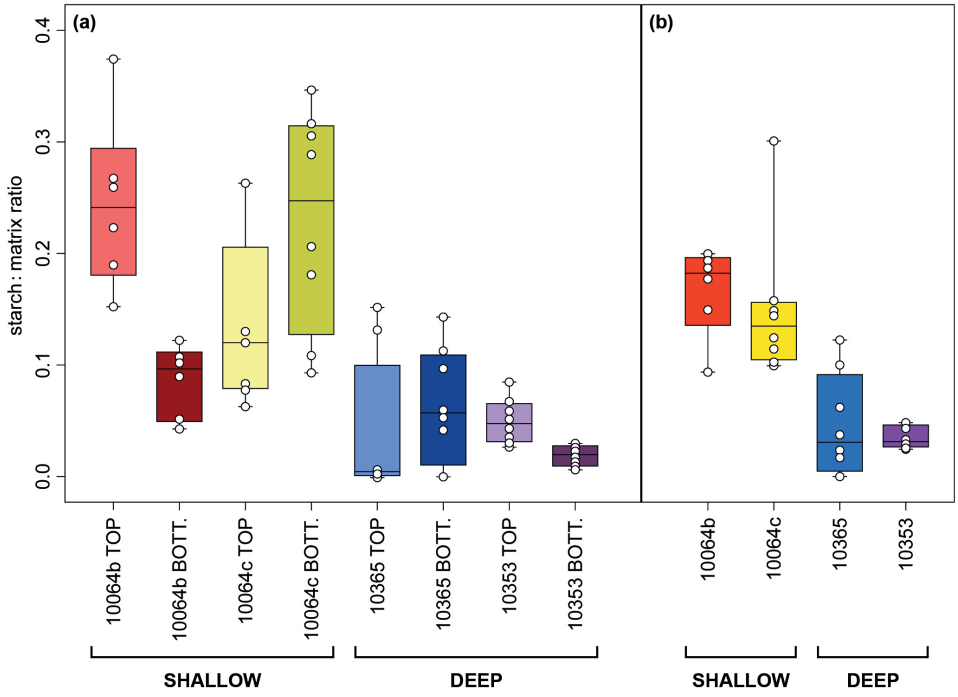

Fig. 4 Boxplots visualizing (a) the distribution of starch:matrix ratios in top and bottom parts of rhodoliths from different water depths (note that differences are only significant in cases where top values exceed bottom values) and (b) the distribution of starch:matrix ratios of complete rhodoliths from different water depths with significant differences between shallow- and deep-water specimens.

Table 5 Results of the Mann–Whitney pairwise post-hoc tests indicating significant differences between the starch:matrix ratios of deep (10365; 10353) and shallow (10064b; 10064c) water rhodoliths. Values report the Mann–Whitney *U*, followed by the *p*. Values in boldface are statistically significant.

	10064b (shallow)	10064c (shallow)	10365 (deep)
10064c (shallow)	14, 0.22	-	-
10365 (deep)	**2, 0.0054**	**4, 0.0038**	-
10353 (deep)	**0, 0.0024**	**0, 0.0009**	29, 0.7972

The other condition that we predicted would have an effect on differences in starch content was the frequency of rhodolith movement. Rhodoliths are moved and turned over by water energy—waves and tidal currents—and by benthic organisms looking for food, and this happens more commonly in shallow water compared to deeper waters at Mosselbukta (Wisshak et al. 2019), resulting in a more even overall exposure and less dieback of all rhodolith parts in the shallow-water rhodoliths (Schlüter et al. 2021).

The more favourable light conditions for rhodolith-forming CCA in shallow waters allow them to store more carbohydrates as starch granules compared to consuming them in respiration than is the case for the deeper-water rhodoliths. However, recent analyses (Voerman et al. 2023) have suggested that mesophotic conditions can be optimal for rhodolith photosynthesis. While mesophotic conditions might not be optimal for growth, there is also no need to devote energy towards photoinhibition strategies. Another point that needs to be considered in terms of starch production is the seasonal fluctuation at the sampling sites. All examined rhodoliths were collected during the beginning of the summer, in June 2016, when it can be expected that rhodoliths have less starch stored compared to the end of summer. In a year-long in situ experiment in Arctic Bay, Canada, Gould et al. (2022) demonstrated that most of the annual growth of *Clathromorphum compactum* occurred during the sea-ice free summer months (54%), arguing that the observed growth during winter (21%) is most likely a consequence of the mobilization of photosynthate stored during the active summer months.

The clusters derived from the K-mean analysis further highlight the importance of different light conditions for starch:matrix ratios in rhodoliths. Interestingly, the fact that there are two clusters for the shallow-water samples and only one for the deeper-water samples suggests that there are more stable conditions in deeper water. As indicated by Wisshak et al. (2019), the hydrodynamics of Mosselbukta are very complex and,

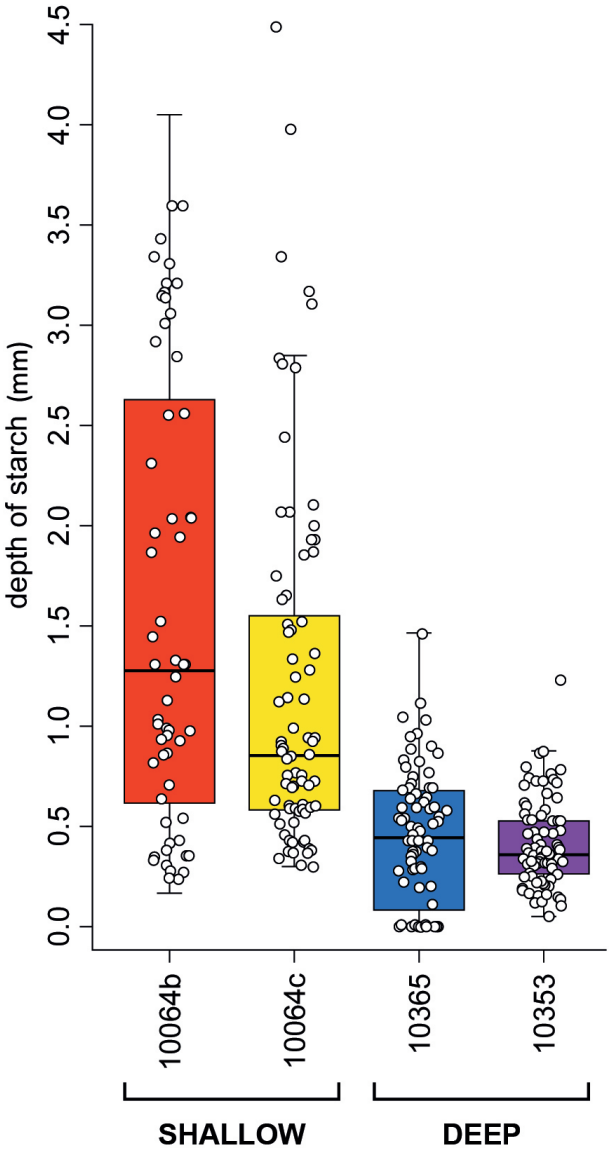

Fig. 5 Boxplots visualizing starch depths in the rhodolith skeleton, indicating a significant difference between shallow- and deep-water rhodoliths. White circles represent individual starch depth measurements.

especially in the shallower areas, are strongly seasonal. The significant differences of starch thickness between shallow- and deep-water samples underline these findings.

As outlined above, rhodoliths are turned more frequently in shallow than in deeper waters (Schlüter et al. 2021) but even at shallow depths rhodoliths periodically remain in a specific position long enough for photosynthesis and starch production to reflect the rhodoliths' orientation. We therefore hypothesized that those parts of the rhodolith facing upwards upon collection should contain more starch than the bottom parts. However, only in half of the samples (10064b and 10353) did the upper parts have a higher starch:matrix ratio than the lower parts. Importantly, the differences were only significant for these two samples, indicating a partial validation of our hypothesis. This rather irregular pattern likely points to a long-term accumulation of starch within the rhodoliths, indicating that not all starch is consumed but may also become buried in the deeper parts of the CCA skeleton.

Table 6 Results of the Shapiro–Wilk test for normal distribution of data for the complete rhodolith starch storage depths.

	10064b complete	10064c complete	10365 complete	10353 complete
n	60	80	80	80
Shapiro–Wilk *W*	0.8915	0.8209	0.6878	0.9333
p (normal)	<0.001	<0.001	<0.001	<0.001
normal distribution	No	No	No	No

Table 7 Results of the Dunn's post hoc test indicating significant differences between the starch storage depths in the complete rhodoliths, indicating significant differences between water depths. Values in boldface are statistically significant.

	10064b (shallow)	10064c (shallow)	10365 (deep)	10353 (deep)
10064b (shallow)		0.3858	**<0.001**	**<0.001**
10064c (shallow)	0.3858		**<0.001**	**<0.001**
10365 (deep)	**<0.001**	**<0.001**		0.2681
10353 (deep)	**<0.001**	**<0.001**	0.2681	

Implications for rhodoliths as blue carbon

Nellemann et al. (2009) introduced the term "blue carbon" to describe carbon buried in marine sediments and to highlight the importance of carbon sequestration in marine ecosystems and its potential role in mitigating climate change. Lovelock & Duarte (2019) established the following criteria for a species or habitat to be considered as blue carbon: significant scale of greenhouse gas emission removals, long-term storage of fixed CO_2 and the potential to be managed or enhanced through practical action.

At present, mangroves, salt marshes and seagrass meadows are considered as the most important blue carbon ecosystems (Lovelock & Duarte 2019). James et al. (2024) conducted a meta-analysis of 253 studies to identify other coastal ecosystems with a strong capacity to act as blue carbon sinks. Among others, the authors identified CCA beds as important in this context. On the one hand, CCA act as a CO_2 sink in the process of

Citation: *Polar Research* 2025, *44*, 10992, http://dx.doi.org/10.33265/polar.v44.10992

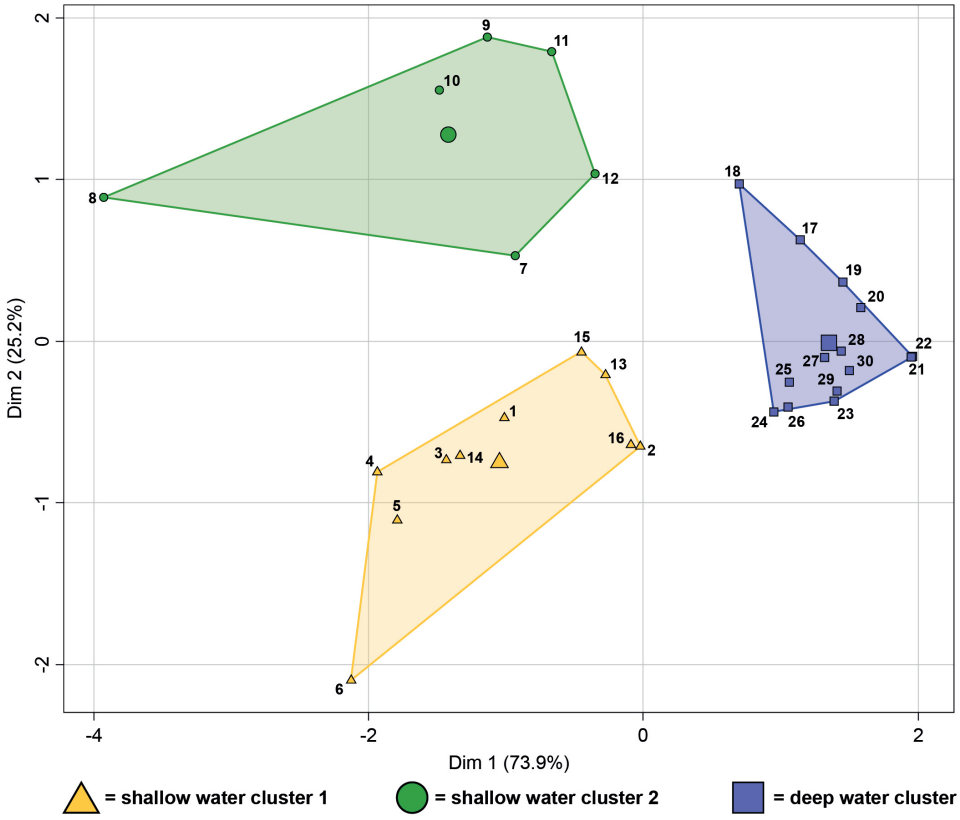

Fig. 6 Clusters of starch:matrix ratios deriving from the K-means analysis. Numbers 1–14 represent shallow-water samples (numbers 1–6 are from specimen 10064b and numbers 7–14 are from specimen 10064c), while numbers 15–30 represent deeper-water samples (numbers 15–22 are from specimen 10365 and numbers 23–30 are from 10353). With the exception of slabs 10365-1 (number 15) and 10365-2.1 (number 16), the deep-water samples are grouped together in one cluster (blue). The shallow-water samples form two different clusters (yellow and green), with each cluster representing a single rhodolith specimen.

photosynthesis and $CaCO_3$ dissolution and weathering. On the other hand, they act as a CO_2 source in the process of respiration and $CaCO_3$ production (van der Heijden & Kamenos 2015). However, carbon sink estimates mostly account for the balance between the CO_2 sequestered and the CO_2 emitted during calcification (Krause-Jensen et al. 2018). Additionally, Mao et al. (2024) showed experimentally that the release of CO_2 from calcification in *Boreolithothamnion soriferum* is considerably less than theoretically predicted, because of internal carbon cycling. The long-term removal of CO_2 requires the fixed carbon to remain stored for 100–1000 years (van der Heijden & Kamenos 2015). The rhodoliths from Mosselbukta clearly fulfil the criteria of longevity (>100 years, Teichert et al. 2024) and, also taking into account their role in carbonate sedimentology (Teichert 2024), they could be considered as potential contributors to the long-term removal of CO_2 up to geological timescales.

The results of our study bring a new aspect to the discussion about CCA and blue carbon by highlighting that the starch is not only located in the superficial tissue of the CCA, but also several millimetres deep in the skeleton. This means it is highly probable that the still-living algae cannot reach the starch and use it for metabolism after the CCA skeleton has reached a specific thickness. It would be useful to find out the thallus depth at which stored starch can still be mobilized by the CCA when needed. Rhodoliths formed by CCA often occur as massive, bed-like formations (Riosmena-Rodriguez et al. 2017). If parts of such beds are buried during, for example, a storm, the starch content is removed from the carbon cycle for the medium- or long-term.

A great deal remains unknown about blue carbon in general, especially the potential role of CCA as a possible carbon sink despite being calcifiers. While rhodoliths have been suggested before as potential blue carbon candidates (Tuya et al. 2023), their high production of $CaCO_3$ might actually lead to a negative CO_2 balance. It has yet to be explored if the amount of CO_2 that is removed from the environment during photosynthesis and dissolution/

weathering exceeds the amount that is released during the calcification process. However, the production and storage of floridean starch could shift the carbon balance towards more CO_2 removal depending on the starch:matrix ratio. Our study provides some basic results on the distribution of starch in rhodoliths and points to its potential for long-term sequestration of CO_2. In this context, it is interesting that starch can be fossilized; the oldest fossilized starch is 280 million years old (Liu et al. 2018). The amount of starch stored inside the living tissue as well as in the skeleton of CCA might contribute to the amount of fixed CO_2 that is removed from the system, and it might outweigh the amount of CO_2 being produced during the process of calcification. Further quantification of buried starch within rhodolith beds would help to determine whether rhodoliths are blue carbon.

Acknowledgements

The authors would like to thank Captain Ralf Schmidt, the crew and the shipboard party of the RV *Maria S. Merian* cruise no. 55. In particular, they acknowledge Karen Hissmann and Jürgen Schauer (both GEOMAR Helmholtz-Zentrum für Ozeanforschung Kiel) for rhodolith sampling and seafloor video documentation with the *Jago* submersible. They are grateful to Christian Schulbert (Friedrich-Alexander-Universität Erlangen-Nürnberg; FAU) for the colouration of the CCA starch scanning electron microscopic image. They also thank Heidi Burdett and an anonymous reviewer for their constructive comments, which improved our manuscript.

Disclosure statement

The authors report no conflict of interest.

Funding

ST and IP were supported by the Dr. Hertha und Helmut Schmauser-Stiftung. Funding for the *Maria S. Merian* cruise 55 was provided to MW by the German Research Foundation in concert with the Leitstelle Deutsche Forschungsschiffe.

Data availability

The data that support the findings of this study are available within the publication. Images created are available from the corresponding author upon request.

References

Adey W.H. 1970. The effects of light and temperature on growth rates in boreal–Subarctic crustose corallines. *Journal of Phycology 6*, 269–276, doi: 10.1111/j.1529-8817.1970.tb02392.x.

Bilan M.I. & Usov A.I. 2001. Polysaccharides of calcareous algae and their effect on the calcification process. *Russian Journal of Bioorganic Chemistry 27*, 2–16, doi: 10.1023/A:1009584516443.

Borowitzka M.A. 1978. Plastid development and floridean starch grain formation during carposporogenesis in the coralline red alga *Lithothrix aspergillum* Gray. *Protoplasma 95*, 217–228, doi: 10.1007/BF01294452.

Bosence D. 1983. Description and classification of rhodoliths (rhodoids, rhodolites). In T.M. Peryt (ed.): *Coated grains*. Pp. 217–224. Berlin: Springer.

Colin J.J. & Gaultier de Claubry H.F. 1814. Sur les combinaisons de l'iode avec les substances végétales et animales. (On combinations of iodine with plant and animal substances.) *Annales de Chimie 90*, 87–100.

Davis H., Skrzypek W. & Khan A. 1994. Iodine binding by amylopectin and stability of the amylopectin–iodine complex. *Journal of Polymer Science Part A: Polymer Chemistry 32*, 2267–2274, doi: 10.1002/pola.1994.080321208.

Fredericq S., Krayesky-Self S., Sauvage T., Richards J., Kittle R., Arakaki N., Hickerson E. & Schmidt W.E. 2019. The critical importance of rhodoliths in the life cycle completion of both macro- and microalgae, and as holobionts for the establishment and maintenance of marine biodiversity. *Frontiers in Marine Science 5*, article no. 502, doi: 10.3389/fmars.2018.00502.

Freiwald A. & Henrich R. 1994. Reefal coralline algal build-ups within the Arctic circle: morphology and sedimentary dynamics under extreme environmental seasonality. *Sedimentology 41*, 963–984, doi: 10.1111/j.1365-3091.1994.tb01435.x.

Gabrielson P.W., Maneveldt G.W., Hughey J.R. & Peña V. 2023. Taxonomic contributions to Hapalidiales (Corallinophycidae, Rhodophyta): *Boreolithothamnion* gen. nov., *Lithothamnion* redefined and with three new species and *Roseolithon* with new combinations. *Journal of Phycology 59*, 751–774, doi: 10.1111/jpy.13353.

Gantt E. 1990. Pigmentation and photoacclimation. In K.M. Cole & R.G. Sheath (eds.): *Biology of the red algae*. Pp. 203–219. Cambridge: Cambridge University Press.

Giraud G. & Cabioch G. 1983. Inclusions cytoplasmiques remarquables chez les Corallinacees (Rhodophytes, Cryptomemiales). (Remarkable cytoplasmic inclusions in Corallinaceae [Rhodophytes, Cryptomemiales].) *Annales des Sciences Naturelles, Botanique 13*, 29–43.

Gould J., Halfar J., Adey W. & Ries J.B. 2022. Growth as a function of sea ice cover, light and temperature in the Arctic/Subarctic coralline *C. compactum*: a year-long in situ experiment in the High Arctic. *Frontiers in Marine Science 9*, article no. 900033, doi: 10.3389/fmars.2022.900033.

Hammer Ø., Harper D.A.T. & Ryan P.D. 2001. PAST: paleontological statistics software package for education and data analysis. *Palaeontologia Electronica 4*, article no.1.

James K., Macreadie P.I., Burdett H.L., Davies I. & Kamenos N.A. 2024. It's time to broaden what we consider a 'blue carbon ecosystem'. *Global Change Biology 30*, e17261, doi: 10.1111/gcb.17261.

Kassambara A. & Mundt F. 2020. *Extract and visualize the results of multivariate data analyses.* R package factoextra version 1.0.7. Accessed on the internet at https://cran.r-project.org/web/packages/factoextra/index.html on 31 January 2024.

Kjellman F.R. 1883. *The algae of the Arctic Sea. A survey of the species, together with an exposition of the general characteristics of the development of the flora. Kongliga Svenska Vetenskaps-Akademiens Handlingar 20*. Stockholm: P.A. Norstedt & Söner.

Krause-Jensen D., Lavery P., Serrano O., Marbà N., Masque P. & Duarte C.M. 2018. Sequestration of macroalgal carbon: the elephant in the blue carbon room. *Biology Letters 14*, article no. 20180236, doi: 10.1098/rsbl.2018.0236.

Littler M.M., Littler D.S., Blair S.M. & Norris J.N. 1985. Deepest known plant life discovered on an uncharted seamount. *Science 227*, 57–59, doi: 10.1126/science.227.4682.57.

Liu F., Bomfleur B., Peng H., Li Q., Kerp H. & Zhu H. 2018. 280-m.y.-old fossil starch reveals early plant–animal mutualism. *Geology 46*, 423–426, doi: 10.1130/g39929.1.

López Correa M., Teichert S., Ragazzola F., Cazorla Vázquez S., Engel F.B., Hurle K., Mazzoli C., Kuklinski P., Raiteri G. & Lombardi C. 2023. Structural and geochemical assessment of the coralline alga *Tethysphytum antarcticum* from Terra Nova Bay, Ross Sea, Antarctica. *Minerals 13*, article no. 215, doi: 10.3390/min13020215.

Lovelock C.E. & Duarte C.M. 2019. Dimensions of blue carbon and emerging perspectives. *Biology Letters 15*, article no. 20180781, doi: 10.1098/rsbl.2018.0781.

MacQueen J. 1967. Some methods for classification and analysis of multivariate observations. In L.M. Le Cam & J. Neyman (eds.): *Proceedings of the Fifth Berkeley Symposium on Mathematical Statistics and Probability. Volume I: Theory of Statistics*. Pp. 281–297. Berkeley: University of California Press.

Maechler M., Rousseeuw P., Struyf A., Hubert M. & Hornik K. 2023. *Cluster: cluster analysis basics and extensions*. Accessed on the internet at https://search.gesis.org/publication/zis-MaechlerRousseeuwStruyfHubertHornikK.2021cluster on 16 December 2023.

Mao J., Burdett H.L. & Kamenos N.A. 2024. Efficient carbon recycling between calcification and photosynthesis in red coralline algae. *Biology Letters 20*, article no. 20230598, doi: 10.1098/rsbl.2023.0598.

Mao J., Burdett H.L., McGill R.A.R., Newton J., Gulliver P. & Kamenos N.A. 2020. Carbon burial over the last four millennia is regulated by both climatic and land use change. *Global Change Biology 26*, 2496–2504, doi: 10.1111/gcb.15021.

Nash M.C., Troitzsch U., Opdyke B.N., Trafford J.M., Russell B.D. & Kline D.I. 2011. First discovery of dolomite and magnesite in living coralline algae and its geobiological implications. *Biogeosciences 8*, 3331–3340, doi: 10.5194/bg-8-3331-2011.

Nellemann C., Corcoran E., Duarte C.M., Valdrés L., Young C.D., Fonseca L. & Grimsditch G. 2009. *Blue carbon: the role of healthy oceans in binding carbon: a rapid response assessment.* Nairobi: United Nations Environment Programme.

NOAA (National Oceanic and Atmospheric Administration) 2023. Sunset table for Mosselbukta 2016: NOAA Global Monitoring Laboratory. Accessed on the internet at https://gml.noaa.gov/grad/solcalc/table.php?lat=79.880089&lon=15.952148 4&year=2016 on 27 November 2023.

Pueschel C.M. 1990. Cell structure. In K.M. Cole & R.G. Sheath (ed.): *Biology of the red algae*. Pp. 7–41. Cambridge: Cambridge University Press.

Pyko I., Wisshak M. & Teichert S. 2025. Depth-related controls on the quantitative composition of rhodolith matrices in the High Arctic. *Aquatic Conservation: Marine and Freshwater Ecosystems 35*, e70045, doi: 10.1002/aqc.70045.

Ragazzola F., Kolzenburg R., Zekonyte J., Teichert S., Jiang C., Zuljevic A., Caragnano A. & Falace A. 2020. Structural and elemental analysis of the freshwater, low-Mg calcite coralline alga *Pneophyllum cetinaensis*. *Plants 9*, article no. 1089, doi: 10.3390/plants9091089.

R Core Team 2023. *R: a language and environment for statistical computing.* Vienna: R Foundation for Statistical Computing.

Riding R., Cope J.C.W. & Taylor P.D. 1998. A coralline-like red alga from the lower Ordovician of Wales. *Palaeontology 41*, 1069–1076.

Riosmena-Rodriguez R., Nelson W. & Aguirre J. (eds.) 2017. *Rhodolith/Maërl beds: a global perspective.* Berlin: Springer.

Saenger W. 1984. The structure of the blue starch–iodine complex. *Naturwissenschaften 71*, 31–36, doi: 10.1007/BF00365977.

Schindelin J., Arganda-Carreras I., Frise E., Kaynig V., Longair M., Pietzsch T., Preibisch S., Rueden C., Saalfeld S., Schmid B., Tinevez J.-Y., White D.J., Hartenstein V., Eliceiri K., Tomancak P. & Cardona A. 2012. Fiji: an open-source platform for biological-image analysis. *Nature Methods 9*, article no. 676, doi: 10.1038/nmeth.2019.

Schlüter M., Pyko I., Wisshak M., Schulbert C. & Teichert S. 2021. Growth interruptions in Arctic rhodoliths correspond to water depth and rhodolith morphology. *Minerals 11*, article no. 538, doi: 10.3390/min11050538.

Smith A.M., Sutherland J.E., Kregting L., Farr T.J. & Winter D.J. 2012. Phylomineralogy of the coralline red algae: correlation of skeletal mineralogy with molecular phylogeny. *Phytochemistry 81*, 97–108, doi: 10.1016/j.phytochem.2012.06.003.

Spreen G., Kaleschke L. & Heygster G. 2008. Sea ice remote sensing using AMSR-E 89-GHz channels. *Journal of Geophysical Research—Oceans 113*, C02S03, doi: 10.1029/2005JC003384.

Straube E., Neumann H., Wisshak M., Mathes G. & Teichert S. 2024. Bayesian analysis of biodiversity patterns via beam trawl versus video transect—a comparative case study of Svalbard rhodolith beds. *Biodiversity and Conservation 33*, 1099–1123, doi: 10.1007/s10531-024-02788-y.

Teichert S. 2013. *Rhodoliths (Corallinales, Rhodophyta) as a biosedimentary system in Arctic environments (Svalbard archipelago, Norway)*. PhD thesis, Dept. of Geography and Earth Sciences, Friedrich-Alexander-Universität Erlangen-Nürnberg, Erlangen.

Teichert S. 2024. Attached and free-living crustose coralline algae and their functional traits in the geological record and today. *Facies 70*, article no. 8, doi: 10.1007/s10347-024-00682-1.

Teichert S. & Freiwald A. 2014. Polar coralline algal $CaCO_3$-production rates correspond to intensity and duration of the solar radiation. *Biogeosciences 11*, 833–842, doi: 10.5194/bg-11-833-2014.

Teichert S., Reddin C.J. & Wisshak M. 2024. In situ decrease in rhodolith growth associated with Arctic climate change. *Global Change Biology 30*, e17300, doi: 10.1111/gcb.17300.

Teichert S., Steinbauer M. & Kiessling W. 2020. A possible link between coral reef success, crustose coralline algae and the evolution of herbivory. *Scientific Reports 10*, article no. 17748, doi: 10.1038/s41598-020-73900-9.

Teichert S., Voigt N. & Wisshak M. 2020. Do skeletal Mg/Ca ratios of Arctic rhodoliths reflect atmospheric CO_2 concentrations? *Polar Biology 43*, 2059–2069, doi: 10.1007/s00300-020-02767-3.

Teichert S., Woelkerling W. & Munnecke A. 2019. Coralline red algae from the Silurian of Gotland indicate that the order Corallinales (Corallinophycidae, Rhodophyta) is much older than previously thought. *Palaeontology 62*, 599–613, doi: 10.1111/pala.12418.

Teichert S., Woelkerling W.J., Rüggeberg A., Wisshak M., Piepenburg D., Meyerhöfer M., Form A. & Freiwald A. 2014. Arctic rhodolith beds and their environmental controls. *Facies 60*, 15–37, doi: 10.1007/s10347-013-0372-2.

Tuya F., Schubert N., Aguirre J., Basso D., Bastos E.O., Berchez F., Bernardino A.F., Bosch N.E., Burdett H.L., Espino F., Fernández-Gárcia C., Francini-Filho R.B., Gagnon P., Hall-Spencer J.M., Haroun R., Hofmann L.C., Horta P.A., Kamenos N.A., Le Gall L., Magris R.A., Martin S., Nelson W.A., Neves P., Olivé I., Otero-Ferrer F., Peña V., Pereira-Filho G.H., Ragazzola F., Rebelo A.C., Ribeiro C., Rinde E., Schoenrock K., Silva J., Sissini M.N. & Tâmega F.T.S. 2023. Levelling-up rhodolith-bed science to address global-scale conservation challenges. *Science of the Total Environment 892*, article no. 164818, doi: 10.1016/j.scitotenv.2023.164818.

Van Dam B.R., Zeller M.A., Lopes C., Smyth A.R., Böttcher M.E., Osburn C.L., Zimmerman T., Pröfrock D., Fourqurean J.W. & Thomas H. 2021. Calcification-driven CO_2 emissions exceed "blue carbon" sequestration in a carbonate seagrass meadow. *Science Advances 7*, article no. 1372, doi: 10.1126/sciadv.abj1372.

van der Heijden L.H. & Kamenos N.A. 2015. Reviews and syntheses: calculating the global contribution of coralline algae to total carbon burial. *Biogeosciences 12*, 6429–6441, doi: 10.5194/bg-12-6429-2015.

Viola R., Nyvall P. & Pedersen M. 2001. The unique features of starch metabolism in red algae. *Proceedings of the Royal Society B: Biological Sciences 268*, 1417–1422, doi: 10.1098/rspb.2001.1644.

Voerman S.E., Marsh B.C., Bahia R.G., Pereira-Filho G.H., Becker A.C.F., Amado-Filho G.M., Ruseckas A., Turnbull G.A., Samuel I.D.W. & Burdett H.L. 2023. Dominance of photo over chromatic acclimation strategies by habitat-forming mesophotic red algae. *Proceedings of the Royal Society B: Biological Sciences 290*, article no. 20231329, doi: 10.1098/rspb.2023.1329.

Wiencke C., Gómez I. & Dunton K. 2009. Phenology and seasonal physiological performance of polar seaweeds. *Botanica Marina 52*, 585–592, doi: 10.1515/BOT.2009.078.

Wisshak M., Bartholomä A., Beuck L., Büscher J., Form A., Freiwald A., Halfar J., Hetzinger S., van Heugten B., Hissmann K., Holler P., Meyer N., Neumann H., Raddatz J., Rüggeberg A., Teichert S. & Wehrmann A. 2017. *Habitat characteristics and carbonate cycling of macrophyte-supported polar carbonate factories (Svalbard.) Cruise no. MSM55. June 11–June 29, 2016. Reykjavik (Iceland)—Longyearbyen (Norway). Maria S. Merian-Berichte*. Bremen: German Research Foundation, Senate Commission on Oceanography.

Wisshak M., Neumann H., Rüggeberg A., Büscher J., Linke P. & Raddatz J. 2019. Epibenthos dynamics and environmental fluctuations in two contrasting polar carbonate factories (Mosselbukta and Bjørnøy-Banken, Svalbard). *Frontiers in Marine Science 6*, article no. 667, doi: 10.3389/fmars.2019.00667.

Woelkerling W.J. 1988. *The coralline red algae*. Oxford: Oxford University Press.

Xue J., Purushotham P., Acheson J.F., Ho R., Zimmer J., McFarlane C., Van Petegem F., Martone P.T. & Samuels A.L. 2021. Functional characterization of a cellulose synthase, CtCESA1, from the marine red alga *Calliarthron tuberculosum* (Corallinales). *Journal of Experimental Botany 73*, 680–695, doi: 10.1093/jxb/erab414.

Yu S., Blennow A., Bojko M., Madsen F., Olsen C.E. & Engelsen S.B. 2002. Physico-chemical characterization of floridean starch of red algae. *Starch—Stärke 54*, 66–74, doi: 10.1002/1521-379X(200202)54:2<66::AID-STAR66>3.0.CO;2-B.

Yu Y., Jia X., Wang W., Jin Y., Liu W., Wang D., Mao Y., Xie C. & Liu T. 2021. Floridean starch and floridoside metabolic pathways of *Neoporphyra haitanensis* and their regulatory mechanism under continuous darkness. *Marine Drugs 19*, article no. 664, doi: 10.3390/md19120664.